AIAA JOURNAL
Vol. 43, No. 8, August 2005

Direct Simulation Monte Carlo Modeling of Homogeneous Condensation in Supersonic Plumes

Jiaqiang Zhong,* Michael I. Zeifman,† and Deborah A. Levin‡
Pennsylvania State University, University Park, Pennsylvania 16802
and
Sergey F. Gimelshein§
University of Southern California, Los Angeles, California 90089

A particle simulation method to model water condensation process in a supersonic rocket plume is proposed and developed. Classic nucleation theory is used to predict nucleation, condensation, and the evaporation rates for water clusters. Microscopic kinetic models are developed to simulate collision processes between water clusters and monomers, between water clusters and foreign molecules, and evaporation of monomers from water clusters. These models are integrated into the direct simulation Monte Carlo method to simulate an axisymmetric multispecies gas expansion coupled with condensation. The developed computational scheme, first verified by empirical scaling laws of condensation in supersonic microjets, is then applied to predict the spatial distributions of water cluster number density, size, and temperature in a rocket exhaust plume. An empirical equation is used to correct classical nucleation rate, condensation results are compared between the original and corrected nucleation rate, and the impact of the nucleation rate on a flow with condensation is discussed in detail.

Nomenclature

A = foreign monomer species
B = condensate monomer species
C = condensation rate
c_p = heat capacity
d = nozzle-throat diameter, or particle diameter
E = evaporation rate or energy
J = nucleation rate
k = Boltzmann's constant
L = latent heat of evaporation
M = cluster mass
m = molecular mass
N = cluster species or number of simulated particles
n = number density
P = pressure
p = vapor pressure
q = sticking coefficient, 1, or constant in scaling law
R = vapor constant, k/m
r = cluster radius
S = degree of supersaturation
T = temperature
V = cluster velocity
$\boldsymbol{V}$ = cluster velocity vector
v = molecular velocity
$\boldsymbol{v}$ = monomer or molecular velocity vector
γ = specific heat ratio
Θ = characteristic temperature
μ = mean spacing between particles
ξ = number of degrees of freedom
ρ = density
σ = surface tension or collision cross section

Subscripts

c = cluster or nucleus species
i = cluster size
int = internal state
m = monomer
r = rotational state
s = saturation state
v = vapor state, or vibrational state
w = liquid state or water
0 = stagnation state
1 = state before a collision
2 = state after a collision
$*$ = critical state

Received 25 March 2004; revision received 2 February 2005; accepted for publication 2 February 2005.

*Graduate Student, Department of Aerospace Engineering. Student Member AIAA.
†Research Associate, Department of Aerospace Engineering. Member AIAA.
‡Associate Professor, Department of Aerospace Engineering. Associate Fellow AIAA.
§Research Assistant Professor, Department of Aerospace and Mechanical Engineering. Member AIAA.

I. Introduction

WHEN a rocket-engine exhaust plume expands into a vacuum or a rarefied background gas, the water vapor in the exhaust flow can become saturated or even supersaturated. In the absence of foreign nuclei, homogeneous condensation[1–3] can occur if supercritical embryos form as a result of a large degree of supersaturation. Once the condensation process begins, it transfers mass from and adds energy to the gas phase, resulting in changes of the flowfield. The changes that occur in the flowfield can result in increased likelihood of plume contamination of spacecraft surfaces as well as affect the observance of high-altitude rocket plumes.

Condensation in freely expanding flows has been studied for many years. Here we mention only a few papers that deal with the modeling of condensation. Assuming a one-dimensional and steady-state nucleation process, Wu[4] predicted the onset of homogeneous water condensation in the exhaust plume of an Apollo engine. Perrell et al.[5] calculated the condensation in a hypersonic wind tunnel by using a finite volume method in an axisymmetric formulation, and showed that the condensation affects the flow temperature, pressure, Mach number, and mass fraction of liquid. Masuda et al.[6] studied the effects of water-vapor condensation in a chemical oxygen-iodine laser and compared the excitation efficiency of oxygen with and without condensation in a one-dimensional calculation.

Most of the papers to date examine the condensation process in ground-based facilities using continuum approaches. There are very

few experimental and theoretical treatments, however, on the condensation in rocket plumes expanding into a rarefied atmosphere at high altitudes. The important feature of these plumes is the strong gradients, especially in the vicinity of the nozzle lip and in the side and backflow of the plume. The flow is characterized by a strong nonequilibrium, and the continuum approach is not strictly applicable. The accurate modeling of such plumes can require another approach, for example, a particle simulation method.

The main objective of the paper is the development of a kinetic particle approach to model the coupled nonequilibrium gas expansion and water condensation processes, and application of this approach to rocket plumes expanding into a highly rarefied atmosphere. The direct simulation Monte Carlo (DSMC) method[7] is chosen as the main computational tool capable of modeling both processes. Originally proposed for rarefied and transitional flows, the DSMC method has recently been applied to model near-continuum and continuum flows. This work presents, to the best of our knowledge, the first application of the method to predict the condensation in rocket plumes.

The process of condensation from the gas phase can be divided into two stages, nucleation of small drops or clusters and their subsequent growth.[8] Whereas it is generally acknowledged that the growth of clusters larger than, say, decamers is satisfactorily described by unimolecular reactions of sticking and evaporation,[9] the process of nucleation from the vapor is still not fully understood. In addition to various thermodynamic theories that relate the formation of a thermodynamically stable nucleus to density fluctuations,[1,10] there are kinetic models in which the nucleus is considered to be a dimer formed in a ternary collision of monomers.[11,12] Even though the kinetic models are more appropriate for DSMC,[13] the lack of reliable data on ternary collisions[11,12] as well as the need for quantitative characterization of various complex reactions among very small clusters and monomers[9] hinders their implementation. On the contrary, the parameters of thermodynamically based nucleation theories are accessible in the literature. Moreover, the corresponding estimated nucleus size usually exceeds 10 molecules for typical conditions in the rocket plume.[14] We choose, therefore, a thermodynamically based nucleation theory to characterize the process of cluster nucleation in the rocket plume.

The paper is organized as follows. Section II justifies the use of the DSMC method for modeling of the coupled condensation flow. Section III briefly reviews classical nucleation theory (CNT), which we use to model the nucleation process. Freshly nucleated water clusters interact with the surrounding molecules and other clusters. The corresponding microscopic models involving cluster interactions to be implemented by the DSMC method are described in Sec. IV. Computational techniques used in the microscopic models are enumerated in Sec. V. In Sec. VI, these models together with the nucleation model are integrated into a DSMC computational scheme. We present various test cases that validate the numerical implementation of this new kinetic approach for the microscopic models. We also present the flow simulations that validate the experimentally derived scaling laws of Hagena and Obert,[15] and we discuss simulation results for a space rocket plume.

II. General Issues Associated with the DSMC Modeling of the Coupled Condensation Flow

The main challenge in modeling coupled condensation flow is posed by the different length and timescales of the processes controlled by the intermolecular interaction and the processes of molecular/cluster transport in the flow. The Brownian motion of molecules in a cluster as well as the interaction of molecules in a collision occur on a timescale of picoseconds, whereas the characteristic timescale for particle transport in a supersonic plume is a microsecond. The only way to address this challenge is to use a relatively accurate model for either scale and a coarse-grained model for the other scale. Because we are mostly interested in processes on the microscale, we will use coarse-grained models for the intermolecular interaction. In the current study we implement models of monomer evaporation and molecule–molecule, molecule–cluster, and cluster–cluster collisions to approximate the intermolecular interactions.

In the basic DSMC procedure, the entire flow volume is divided into cells and filled with simulation particles that represent real molecules and clusters. The cell size is defined by the local mean free path, and the number of the simulation particles representing a given species (molecular species or clusters) in the cell is defined as the ratio of the number of real particles to Fnum (the number of real particles represented by a simulated particle). Each simulated molecule is characterized by spatial coordinates, velocity, internal energy, and species-related mass. The simulated clusters are, in addition, characterized by the number of molecules they comprise. The basic principle of DSMC is that the continuous process of particle movement and interaction is uncoupled. First, at each time step every particle is moved according to its velocity. Next, the interaction between the particles is modeled by appropriate coarse-grained models, for example, by collision models. Therefore, the DSMC time step should be chosen such that the particles move only a fraction of the cell size during the time step.

The validity of the DSMC method is related to the requirement of a dilute gas/binary collisions and molecular chaos assumptions. The assumption of a dilute gas implies that only a very small proportion of space is occupied by the particles, and each particle, for the most part of its trajectory, is moving outside the range of influence of other particles. This assumption means that

$$d \ll \mu \tag{1}$$

where μ is related to the gas number density n as

$$\mu = 1/n^{\frac{1}{3}} \tag{2}$$

Three types of interactions exist in the DSMC model: 1) molecule–molecule (M–M) collisions, 2) molecule–cluster (M–C) collisions, and 3) cluster–cluster (C–C) collisions. To understand whether Eq. (1) is satisfied, let us examine the DSMC conditions along the core flow of rocket plume (to be discussed in Sec. VI.C). Because the molecular number density is less than 10^{21} molecules/m^3, previous experience tells us that the DSMC assumptions are easily satisfied for M–M collisions. The mean molecular distance for M–C collisions μ is on the order of or less than 10^{-7} m, whereas for C–C collisions μ is on the order of or less than 10^{-6} m. To evaluate M–C and C–C collisions, we use a cluster diameter d of 10^{-8} m. This corresponds to a cluster size of approximately 100,000 monomers, which is much larger than the maximum size of 500 observed in our simulations. The maximum ratio d/μ calculated for the core flow is 0.02; therefore, the considered molecule–cluster flow is indeed dilute.

The assumption of binary collisions or, more precisely, binary interactions is directly related to the length scales and timescales of the processes in the coupled condensation flow. Molecular dynamics calculations suggest that the duration of a collision between a molecule/cluster and another molecule or a cluster is of the order of 10^{-10}–10^{-12} (Refs. 16 and 17), whereas the estimated mean time between collisions in the considered plume flow is at least 10^{-7} s. The probability of the collision overlap during the DSMC time step is, therefore, negligibly small such that the binary collision assumption holds in our case. In conclusion, the DSMC method is applicable to treat all collisions among clusters and molecules in the rocket plume and other cases, discussed in Sec. VI.

A potential problem could arise in modeling evaporations if the time between subsequent evaporations from the same cluster were small compared to the DSMC time step. Our estimations, however, show that even the maximum observed evaporation rate, of the order of 10^5 molecules per second, corresponds to the mean time to evaporation being significantly larger than the DSMC time step (10^{-7} s).

Finally, we would like to pay special attention to the nucleation process, which to the best of our knowledge has not been modeled in the DSMC. As it was mentioned in the Introduction, the nucleation phenomenon is still not fully understood. A popular view of nucleation as a density fluctuation implies that several monomers must collide simultaneously to form a thermodynamically stable nucleus. Not only is the probability of such multibody collisions

extremely low, but strictly speaking the multibody interactions are prohibited in DSMC. The CNT, outlined in the following section, considers instead a chain of unimolecular reactions of sticking and evaporation that sequentially results in the formation of the nucleus. Even though the derived by CNT nucleus size and nucleation rate have been confirmed in numerous experiments and simulations, the chain of the unimolecular reactions that starts from dimer formation in binary monomer collisions might not realistically represent the detailed mechanism of nucleation. Dimers can not be formed in binary collisions of monomers unless there is an energy loss mechanism such as the interaction with a third monomer.[18]

If we are to use CNT, we, therefore, have little choice but to model nucleation in DSMC as a sudden conversion of a specific number of simulated monomers into the nucleus cluster. This model is approximate, but because the nucleation rate is orders of magnitude lower than the collision rate[14] the possible participation of the simulated monomers in a variety of reactions that eventually resulted in the nucleus formation can be neglected as being very rare. Because our DSMC calculations show that the abundance of nuclei is low (nuclei constitute about 1% of the overall mass of the plume), we believe that these approximations will not affect significantly the distributions of monomers, large clusters, and the overall plume density and temperature.

III. Homogeneous Nucleation Theory

Several versions of thermodynamically based homogeneous nucleation theory have been reported in the literature.[19–22] One of its earliest versions, CNT,[1–3] has remained the most popular, even though it has often been criticized for the bulk description of small clusters[21] and the negligence of the nucleus rotational and translational degrees of freedom.[22] The reasons for the popularity of CNT are that 1) the nucleation rate, that is, the number density of freshly formed clusters per unit time, predicted by CNT fits the experimental data[23,24] much better than the CNT counterparts, and 2) the required parameters for the nucleation and evaporation rates are accessible in the literature. We choose, therefore, the classical nucleation theory[1–3] to model the nucleation of argon[24] and water[4,6] clusters.

According to CNT, embryos of various sizes are formed as a result of density fluctuation processes in a supersaturation vapor. There is an energy barrier, however, in the formation of a cluster, which is related to the cluster surface tension: the free energy loss from the transition of i gas molecules into the liquid phase is overcompensated by the energy increase due to the surface tension. The maximum of this energy barrier occurs at a certain cluster size i_*, which is regarded by CNT as the "critical size"; for clusters larger than i_*-mers, the further growth is thermodynamically favorable, whereas clusters smaller than i_*-mers are thermodynamically unstable. Approximating a cluster by a sphere, the CNT provides the following relation between the radius of the critical size cluster r_*, the surface tension per unit area σ, mass density of the liquid phase ρ, temperature T, and the degree of supersaturation S:

$$r_* = \frac{2\sigma}{\rho_w RT \ln S} \tag{3}$$

Here, R is the ideal-gas constant.

The growth and shrinkage of clusters can occur in various ways. The CNT assumes that both processes proceed with one monomer at a time, that is, by the attaching of a monomer to a cluster and by the evaporation of a monomer from a cluster, correspondingly. The rate of monomer attaching, or condensation rate, can be approximated by the number of water monomers colliding with the cluster times the sticking coefficient q per unit time. The sticking coefficient is defined as the probability of a sticking collision between a cluster and molecule. For an ideal gas we have

$$C = \frac{4\pi r^2 qp}{(2\pi mkT)^{\frac{1}{2}}} \tag{4}$$

The evaporation rate E of a cluster is derived in CNT from the condensation rate assuming that at the critical cluster size the evaporation and condensation rates are equal. That is, the evaporation rate of a cluster of a given size is set equal the condensation rate C of that cluster, as if it were the critical size in the surrounding vapor:

$$E = \frac{4\pi p_s r^2}{(2\pi mkT)^{0.5}} \exp\left(\frac{2\sigma}{\rho RTr}\right) \tag{5}$$

Based on the condensation and evaporation rates given by Eqs. (4) and (5), respectively, and assuming a steady-state condition, one ultimately arrives at the following expression for the nucleation rate J of clusters:

$$J = \left(\frac{2\sigma}{\pi m^3}\right)^{\frac{1}{2}} \frac{\rho_v^2}{\rho_w} \exp\left(\frac{-4\pi r_*^2 \sigma}{3kT}\right) \tag{6}$$

In Eqs. (4–6), T is the temperature of the gas, assumed in CNT also to be the temperature of the cluster. The CNT formulas, Eqs. (4–6), provide a basis for the microscopic kinetic models to be implemented in the DSMC method. Note that in the actual DSMC simulations thermal equilibrium between the cluster and gas is not assumed.

Because of the uncertainty of small cluster surface tension, especially at low temperatures, a discrepancy of several orders of magnitude between the CNT nucleation rate and experimental rate can be observed.[23–26] Recently, an empirically corrected water nucleation rate[27] has been proposed on the basis of experimental measurement in a novel, nucleation pulse chamber.[28] In Sec. VI.C, the corrected nucleation rate for water will be applied, and its impact on the condensation in rocket plumes will be discussed.

IV. Microscopic Kinetic Models to Be Used in DSMC

A particle simulation method, the DSMC,[7] is chosen in the present work to model the condensation process coupled to the multispecies gas expansion. As was discussed in Sec. II, the DSMC method is well documented in the literature, and its applicability is based on the dilute gas and the molecular chaos assumptions. To implement the method for the simulation of condensation in rocket plumes, we need to characterize the following processes: 1) binary collisions among the molecules in the plume, 2) nucleation of new water clusters, 3) interactions between water clusters and water molecules (known as condensation), 4) interactions between water clusters and foreign molecules (to be referred to as nonsticking collisions), 5) evaporation of molecules from clusters, and 6) interactions between clusters. Process 6 has been found to be rare in this work (Sec. VI.C) such that the interaction between clusters has been reduced to the elastic collisions.

In the development of the microscopic models, we proceed from the assumption that all models must be mutually consistent. The most difficult process to be modeled is the process of nucleation. Therefore, having selected CNT to model nucleation, all other models must be consistent with it. In particular, this implies that because CNT uses bulk material properties for the cluster description, we will also use the bulk properties to characterize cluster cross sections, energy, etc., even though there are more accurate methods for cluster characterization.[29]

Next we outline the models characterizing each of these processes. In the remainder of the paper, we will discuss simulation particles, which represent either molecules or clusters.

A. Molecular Collisions

To characterize the monomer-monomer collisions in DSMC, the variable-hard-sphere (VHS) model[7] is used. It assumes that the total collision cross section depends on the relative collision velocity and the scattering interaction can be modeled as a hard sphere. The Larsen–Borgnakke model[7] is employed to characterize the redistribution of the total collision energy among the translational and internal modes of the colliding molecules. For a diatomic molecule, the number of degrees of rotational freedom $\xi_r = 2$; for a polyatomic molecule that comprises three or more atoms, $\xi_r = 3$, except that CO_2 has $\xi_r = 2$ because of its linear structure. The effective number

of degrees of vibrational freedom ξ_v at temperature T is[7]

$$\xi_v = \frac{2\Theta_v/T}{\exp(\Theta_v/T) - 1} \tag{7}$$

where Θ_v is a characteristic vibrational temperature. According to the model, the postcollision values of the kinetic and internal energies are sampled from the local equilibrium distributions with regard to the total collision energy and the number of degrees of freedom.

B. Nucleation

According to CNT, the rate of formation of freshly nucleated clusters, or nuclei J, is given by Eq. (6). Similarly to other investigators,[5,6] we assume that the fresh nuclei are created at the critical size, as determined by the surrounding vapor, Eq. (3), while the same number of vapor monomers are removed to satisfy mass conservation.

Following CNT, we assume that a nucleus is at thermal equilibrium with the surrounding gas. Thus, the translational energy of a nucleus is obtained by sampling the local gas equilibrium distribution given by the local translational temperature and flow velocity of the monomers in the cell. Because CNT assumes that the clusters have properties of the bulk material, we characterize the internal energy of a nucleus in terms of the specific heat capacity of the bulk material (water) c_p as

$$E_{\text{int}} = c_p M_i T_c \tag{8}$$

where i is the number of molecules in the nucleus, T_c is the cluster temperature that initially is assumed to be the local gas translation temperature, and M_i is the cluster mass. In addition to the internal energy E_{int} that characterizes the Brownian motion of molecules inside the cluster at nonzero temperature, clusters also possess binding energy that ties the molecules together. The binding energy per molecule is on the same order as the well depth of the Lennard–Jones potential, $10^{-21}J$, while the internal energy per molecule, Eq. (8), is on the order of $10^{-20}J$. Therefore, in the microscopic models we neglect the change in binding energy caused by the change of cluster size.

C. Condensation or Sticking Collisions

Following CNT, we assume that all interactions between water clusters and water molecules involve either sticking collisions, referred to here as condensation, or evaporation of water molecules from clusters. As was discussed in Sec. II, a cluster of i molecules is assumed to collide with one monomer at a time, so that the condensation process is expressed as

$$N_i + B_1 \rightarrow N_{i+1} \tag{9}$$

Mass conservation is obtained for each sticking collision by removing the sticked molecule from the computational domain, while increasing the cluster size from i to $i+1$. The kinetic and internal energy of the new cluster can be derived from the conservation equations. The total precollision energy includes the monomer kinetic and rotational energies, and cluster-N_i kinetic, and internal energies, whereas the postcollision energy includes the kinetic, and internal energies of cluster-N_{i+1}. The conservation equations are

$$m\boldsymbol{v}_1 + M_i\boldsymbol{V}_i = M_{i+1}\boldsymbol{V}_{i+1} \tag{10}$$

$$\tfrac{1}{2}mv_1^2 + E_r + \tfrac{1}{2}M_i V_i^2 + c_p M_i T_{c,1} = \tfrac{1}{2}M_{i+1}V_{i+1}^2 + c_p M_{i+1} T_{c,2} \tag{11}$$

Note that E_r, the monomer rotational energy, is given by

$$E_r = \tfrac{1}{2}\xi kT \tag{12}$$

The calculation of E_r will be discussed further in the next subsection.

The potential contribution of water monomer vibrational energy has not been included in Eq. (11). The water molecular vibrational characteristic temperatures[30] is 2290 K, which is high compared to the plume gas temperature (less than 200 K). Thus, water molecular vibrational models are inactive for the plume conditions considered here, and the water molecular vibrational energy can be neglected in Eq. (11).

D. Nonsticking Collisions Between Clusters and Monomers

Unlike the sticking collisions between water clusters and water molecules, we regard the collisions between water clusters and foreign molecules as nonsticking collisions[5]:

$$N_{i,1} + A_1 \rightarrow N_{i,2} + A_2 \tag{13}$$

where subscripts 1 and 2 refer to pre- and postcollisional states, and the cluster size index is suppressed because it remains the same in the nonsticking collisions. This process must satisfy momentum and energy conservation:

$$m\boldsymbol{v}_1 + M_1\boldsymbol{V}_1 = m\boldsymbol{v}_2 + M_1\boldsymbol{V}_2 \tag{14}$$

$$E_{r(v),1} + \tfrac{1}{2}mv_1^2 + \tfrac{1}{2}MV_1^2 + c_p MT_{c,1} = E_{r(v),2} + \tfrac{1}{2}mv_2^2 + \tfrac{1}{2}MV_2^2 + c_p MT_{c,2} \tag{15}$$

The term $E_{v,1}$ and $E_{v,2}$ in Eq. (15) refers to nonwater monomer species vibrational energy. Similarly to water, it is assumed that these vibrational energies can be neglected.

The number of unknowns (the postcollision energies and velocities of the cluster and the monomer) in Eqs. (14) and (15) exceeds the number of equations. One possible way to solve these equations could be the use of the Larsen–Borgnakke model,[7] in which the postcollision energies are sampled from the equilibrium distributions with regard to the corresponding numbers of the effective degrees of freedom and the total collision energy. This model has been found effective when the numbers of degrees of freedom of the colliding particles are known and comparable. In the case of a collision between a large cluster and a molecule, the Larsen–Borgnakke model can be computationally unfeasible. Moreover, the effective number of cluster degrees of freedom is generally unknown. To overcome this obstacle, we approximate a collision between a molecule and a large cluster as a molecule-surface interaction.[7] In the simplest case of a diffuse, nonsticking collision with complete thermal accommodation,[7] the postcollision rotational and relative kinetic energies of the molecule are defined by the cluster temperature.

Because the number of molecule–molecule collisions is relatively high compared to the number of cluster-molecule collisions, we can use the mean collisional energies without sampling them from the corresponding distributions. Thus,

$$E_{r(v),2} = \tfrac{1}{2}\xi_{r(v)} kT_{c,1} \tag{16}$$

where ξ is the number of monomer degrees of freedom and the difference between the cluster temperatures before and after the collision is supposed to be small. The mean postcollisional kinetic energy of the molecule in the center of mass system is given by $2kT_1$ in the hard-sphere approximation.[7]

E. Evaporation

Following CNT, we assume that only one monomer at a time can evaporate from a cluster. This process can be expressed as

$$N_i \rightarrow N_{i-1} + A \tag{17}$$

Opposite to the condensation process, the evaporated molecule is added to the computational domain, while the cluster size decreases from i to $i-1$ in each evaporation event. In the evaporation process, the monomer gains translational and rotational energy, reducing the temperature of the original N_i cluster. Momentum and energy conservation require that

$$M_i\boldsymbol{V}_1 = m\boldsymbol{v}_2 + M_{i-1}\boldsymbol{V}_2 \tag{18}$$

$$\tfrac{1}{2}M_i V_1^2 + c_p M_i T_{c,1} = E_r + \tfrac{1}{2}mv_2^2 + \tfrac{1}{2}M_{i-1}V_2^2 + c_p M_{i-1} T_{c,2} \tag{19}$$

Because in CNT the evaporated molecule is in the thermal equilibrium state with the original cluster, its rotational energy E_r is given by $\frac{1}{2}\xi kT_{c,1}$, and that the kinetic energy of the evaporated molecule [second term on the right-hand side (RHS) of Eq. (19)] in the center of mass system is given by $2kT_{c,1}$. The rate of the evaporation process is defined by cluster size and internal temperature in accordance with Eq. (5).

V. Computational Method

The microscopic models of particle interactions described in the preceding section are integrated into the standard DSMC procedure. The specific numerical implementation is discussed next.

Molecular collisions are modeled according to the basic DSMC procedure. The parameters of the VHS collision model are taken from Ref. 7. The number of rotational degrees of freedom used in the Larsen–Borgnakke model of energy redistribution is zero for an atomic gas and two or three for diatomic and polyatomic molecules, respectively. Clusters are modeled as ideal hard spheres of radius r_i as

$$r_i = i^{\frac{1}{3}} r_{\text{ref}} \tag{20}$$

where i is the number of molecules in the cluster and r_{ref} is the reference radius of the cluster molecule given by Ref. 7. Note that for small clusters, Eq. (20) might need to be corrected[13] to account for the molecular distance within a cluster. The frequencies of molecule–cluster and cluster–cluster collisions are calculated according to the basic DSMC theory, as was justified in Sec. II.

Nucleation is modeled by adding a number of new cluster particles into a DSMC cell at each time step. The number of the cluster particles is calculated based on the nucleation rate J, Eq. (6), the time step, the cell volume, and the number of real clusters represented by a simulated cluster particle. The initial clusters are assumed to be created at the critical size for the temperature and pressure conditions in the given cell in accordance with Eq. (3). The initial cluster location is chosen at random within the cell, and the initial cluster flow velocity components and internal temperature are defined based on the corresponding cell values of the monomers. During subsequential time steps, these new cluster particles experience sticking and nonsticking collisions with gas species, as well as evaporation processes, leading to changes of cluster size, internal and binding energies, velocity, and position.

Condensation is modeled by sticking collisions between clusters and molecules of the same material as is explained in Sec. IV.C. The sticking coefficient in the condensation model is assumed to be unity in this work.

Nonsticking collisions are modeled in a manner similar to molecular collisions, as was discussed in Sec. IV.D. The Larsen–Borgnakke model is used to assign internal energy based on the number of degrees of freedom.

Finally, evaporation is modeled by replacing a parent cluster N_i by the child one N_{i-1} and adding a new monomer as is explained in Sec. IV.E. The location of the child cluster coincides with that of the parent cluster, and the location of the evaporated monomer is chosen at random within the cell. The energies of the new particles are assigned based on Eq. (20). At each time step, the time to possible evaporation of each cluster is calculated according to the evaporation rate, Eq. (5). If the calculated time is smaller than the time remaining during the DSMC time step, the evaporation event is accepted, the cluster time is advanced by the calculated time, and this procedure continues until no remaining cluster time within the time step is left. If the calculated time to evaporation is larger than the remaining time, the probability of the evaporation is assessed by the acceptance-rejection method based on the ratio of these two times.

VI. Results

The developed kinetic models are examined using specially designed one-dimensional test cases dealing with condensation, evaporation, and nonsticking collision processes separately. Section VI.A presents comparisons between the numerical DSMC simulation results of the test cases with analytical solutions. In Sec. VI.B, the proposed computational method and physical models are shown to successfully reproduce the well-known scaling laws for the cluster formation in supersonic microjets. Finally, the developed computational method is applied to study the condensation in exhaust rocket plumes, and the results are reported in Sec. VI.C. The DSMC results are based on the SMILE[31] code, extended to include the microscopic models, as discussed earlier.

A. Test Cases

The integration of the microscopic models into the SMILE DSMC code is technically challenging because of the use of the weighting factors, different types of collisions, and parallelization. Three simplified test cases were undertaken to check simulation results against analytic expressions.

To test the condensation model, water clusters are studied in an idealized pure water-vapor environment. For this test case, the evaporation and nucleation processes are turned off artificially, and there are no nonsticking collisions caused by the absence of foreign monomers. The initial water clusters consisting of 50 monomers, at a temperature of 160 K and a velocity of 2000 m/s, are introduced from the left boundary into the vapor environment, which has the same temperature of 160 K and velocity of 2000 m/s. These values are typical for the condensation in a rocket plume (see Sec. VI.C). Note that these cluster conditions are only used here to validate the sticking collision or condendensation model in a vapor environment. In Secs. VI.B and VI.C, we return to Eq. (6) to generate all nuclei. The cluster and water-vapor number densities are 10^{13} and $10^{21}/\text{m}^3$, respectively. The number of real molecules represented by simulated molecules, Fnum, is 2×10^{15} in the simulation, and the species weighting factor[7] for clusters is 1×10^{-8}. Thus, the number of simulated particles representing clusters almost equals the number of particles representing water molecules. Approximately 1 million total simulated molecules are used. Because the cluster number density is much less than the water-vapor number density, the decrease of water-vapor number density due to the condensation process can be neglected. Thus, the condensation process as modeled in these test cases has no impact on the water-vapor environment. The simulations discussed in this section use a time step of 5.0×10^{-8} s and sample the macroparameters from the 20,000th to the 200,000th time step.

The analytical solution of the cluster size growth in the constant vapor environment per time step is defined by Eq. (21):

$$\Delta G = n_v \sigma V_r \Delta t \tag{21}$$

where σ is the collision cross section of the cluster-monomer pair, V_r is its relative velocity, Δt is the time step, a sticking coefficient of 1 is assumed, and n_v is the number density of the monomer vapor. The quantity ΔG represents the new number of vapor molecules that have become attached to the cluster during a single time step. The conservation equations (10) and (11) are solved at the same time for each collision to calculate the increment of cluster temperature and velocity, where the vapor velocity $\boldsymbol{v}_1$ equals thermal velocity plus the flow velocity.

The DSMC simulation results are compared with the analytical solutions, as shown in Fig. 1. From Fig. 1, we can see that DSMC simulation results agree well with the analytical solutions. The results show that the size of the cluster increases slowly at the beginning because of the relatively small collisional cross section, and the rate of cluster temperature increase is quick because of the relatively high latent heat release for small clusters. However, the cluster size increases as the condensation process proceeds, which, in turn, leads to a larger collisional cross section, a quicker growth rate, and a more gradual cluster temperature increase due to the increasing cluster heat capacity.

To test the nonsticking collision model, or the reflection model, water clusters were studied in a pure nitrogen gas environment. Here the evaporation process of the clusters is again artificially turned off, and there is no condensation process due to the absence of water-vapor monomers. The initial water clusters consisting of 300 monomers have a temperature of 200 K and a velocity

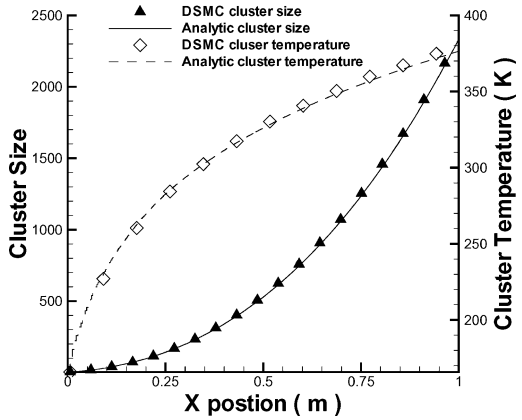

Fig. 1 Comparison of DSMC simulation results and analytical solutions of a one-dimensional condensation process.

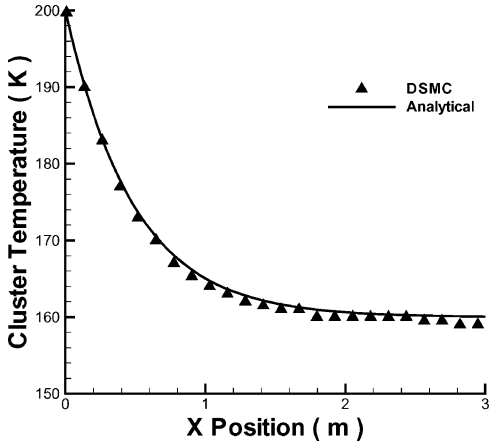

Fig. 2 Comparison of a DSMC simulation result and an analytical solution of a one-dimensional nonsticking collision process.

of 2000 m/s, and the nitrogen gas has a temperature of 160 K and a flow velocity of 2000 m/s. The cluster number density in the simulation is $10^{13}/m^3$, and the nitrogen number density is $10^{21}/m^3$. Here, the same simulation parameters such as Fnum, species weighting factors, and number of the simulated molecules are used as in the condensation test case. Because the nitrogen number density is much larger than the cluster number density, only a small fraction of nitrogen molecules has the chance to collide with the clusters. Thus, the reflection process should have no effect on the nitrogen environment.

The analytical solution of the water cluster temperature is determined as follows. First, the number of collisions between the cluster and the nitrogen monomers is calculated per time step according to the RHS of Eq. (21). Then for each collision, the momentum and energy conservation relationships, Eqs. (14) and (15), are solved, where the monomer velocity before the collision is determined in the same manner as in the condensation test case. The monomer velocity after the collision is modeled by reflection from a diffuse surface at the temperature of the cluster.

The DSMC simulation results are compared with the analytical solution, as shown in Fig. 2. Figure 2 shows that DSMC simulation results are in a good agreement with the analytical solutions of the reflection process in this case. We can see that initially the cluster temperature decreases quickly because of the large temperature difference between the cluster and gas. The relatively cooler gas is able to carry away more cluster internal energy. The cluster reaches a final steady-state temperature equal to the gas temperature as the energy exchange between the cluster and gas ceases.

To test the evaporation model, water clusters only are introduced into the computational domain. The same Fnum was used in this case as that half-million simulated particles are used to model water clusters. The initial water clusters consist of 300 monomers, have a

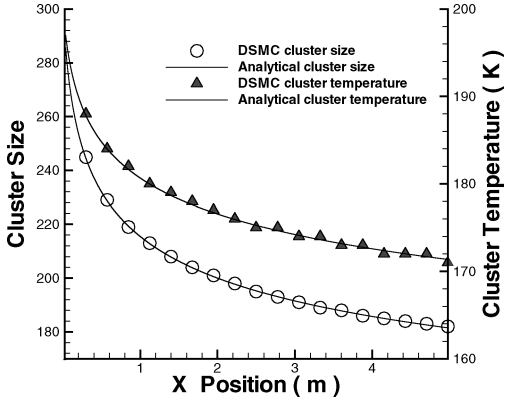

Fig. 3 Comparison of DSMC simulation results and analytical solutions of a one-dimensional evaporation process.

temperature of 200 K, and have a velocity of 2000 m/s. To obtain the analytical solution, the evaporation rate, Eq. (5), is solved first at each time step to calculate the new cluster size, then energy and momentum conservation equations (20) and (18) are solved to calculate the cluster new temperature. Thus, the analytical solutions of cluster size and temperature are obtained at each time step as a function of cluster position.

The one-dimensional evaporation DSMC simulation results are compared with the analytical solution in Fig. 3, and a reasonable agreement is observed. Here, we can see that initially the evaporation rate is large due to the high temperature of the clusters, and the reduction of temperature is also large because the evaporating monomers take away more internal energy due to higher cluster temperature and evaporation rate. As the cluster temperature decreases, the decrease of cluster size becomes slower because of a lower evaporation rate at low cluster temperature, and the decrease of cluster temperature shows the same trend.

B. Scaling Laws

In the past few decades, many experimental studies of condensing flows have been conducted. Most of these experiments, for example, Refs. 32 and 33, are related to a low-speed expansion into a background gas. It is difficult to use these data to verify the developed DSMC scheme due to the low flow velocity, small Knudsen number, and large terminal cluster sizes, which increases the computational cost. However, as early as in 1970s the expansion of supersonic jets into vacuum has been studied extensively. We refer here to the well-known experiments of Hagena who established empirical scaling laws for homogeneous condensation in such jets.[15] Because these scaling laws are often cited in the literature,[18,34] we will use them to validate our numerical model.

According to Hagena, the mean terminal cluster size remains constant if the stagnation pressure and nozzle-throat diameter d satisfy the relationship:

$$P_0 d^q = \text{const} \tag{22}$$

and the stagnation pressure P_0 and stagnation temperature T_0 fall into the range between

$$P_0 T_0^{\gamma/(1-\gamma)} = \text{const} \tag{23}$$

and

$$P_0 T_0^{(1.5\gamma-1)/(1-\gamma)} = \text{const} \tag{24}$$

where constant q is about 0.8 for argon.

Sonic convergent nozzles, similar to those originally used by Hagena, are modeled in the present work to test the condensation/DSMC model. For each nozzle, the convergent angle is 30 deg, and the distance from the nozzle inlet to the throat (outlet) equals the throat radius. Pure argon gas first accelerates in the convergent nozzle, reaches sonic velocity at the throat position, and then expands into vacuum. Table 1 provides nozzle-throat diameter d, stagnation

Table 1 DSMC simulation numerical parameters and terminal mean cluster size of the scaling law P_0 vs d relationship[a]

d, mm	P_0, Pa	Fnum	W	N_m	N_c	Z
0.14	4.0×10^4	2.0×10^6	5.0×10^{-5}	1.30×10^6	0.43×10^6	486
0.70	1.10×10^4	5.0×10^6	5.0×10^{-6}	1.17×10^6	0.52×10^6	524
1.40	5.52×10^3	3.0×10^8	5.0×10^{-7}	0.98×10^6	0.32×10^6	508
2.10	3.50×10^3	5.0×10^8	1.5×10^{-7}	0.94×10^6	0.37×10^6	487
2.80	2.70×10^3	1.0×10^9	1.0×10^{-7}	1.23×10^6	0.41×10^6	518

[a]A value of surface tension, $\sigma = 0.0148$ N/m for an argon cluster was used in all simulations.

Table 2 DSMC simulation numerical parameters and terminal mean cluster size of the scaling law P_0 vs T_0 relationship

T_0, K	P_0, Pa	Fnum	W	N_m	N_c	Z
150	3.26×10^4	4.0×10^6	5.0×10^{-5}	0.60×10^6	0.41×10^6	480
167	3.26×10^4	2.0×10^6	5.0×10^{-5}	1.30×10^6	0.43×10^6	486
180	5.30×10^4	8.0×10^6	5.0×10^{-5}	0.42×10^6	0.31×10^6	466
200	6.90×10^4	8.0×10^6	5.0×10^{-5}	0.48×10^6	0.34×10^6	453
230	9.79×10^4	8.0×10^6	5.0×10^{-5}	0.61×10^6	0.39×10^6	460

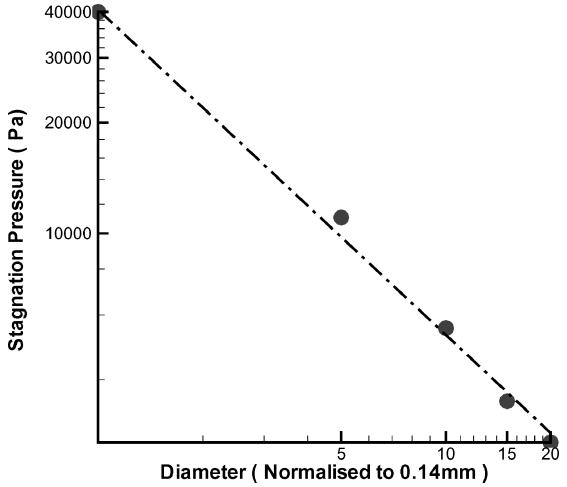

Fig. 4 Comparison of DSMC simulation conditions (●) with the scaling law, Eq. (22) (–·–·–·), $T_0 = 167$ K.

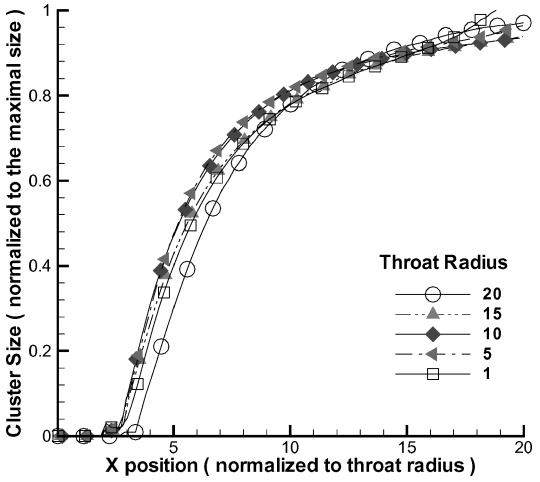

Fig. 5 Cluster growth along the centerline of the DSMC simulations, with the conditions shown in Fig. 4.

pressure P_0, and DSMC numerical parameters used to evaluate the scaling law, Eq. (22). Likewise, Table 2 provides the conditions for the scaling law, as given by Eqs. (23) and (24). In both tables, column Fnum is the number of real molecules represented by a simulated particle, column W represents the species weighting factor for the simulated clusters, N_m and N_c represent the number of simulated molecules and clusters, and Z represents the maximal cluster size at the centerline in the DSMC simulations. For each case, a Navier–Stokes solver, GASP,[35] is first used to obtain the flowfield solution in the nozzle, as well as in the region downstream of the nozzle throat, where the flow is in a state too dense to model with DSMC. Based on the continuum solution, a starting surface is constructed in the undersaturated region, where the Mach number is usually below 2.5. Finally, the developed DSMC simulation scheme is implemented for the region beyond the starting surface. The thermal properties of argon gas are obtained from Ref. 36. The DSMC computational domain for each case extends $2d \times 10d$ with 80×400 cells in radial and axial directions respectively, where d refers to the throat diameter of the convergent nozzle. Each cell can be divided into up to 20 subcells during the simulation. A time step of 1.0×10^{-9} s is used, and a cluster species weighting factor of 5.0×10^{-5} is used in the simulations. The DSMC simulation samples the macroparameters from the 24,000th to the 200,000th time step.

It is seen in Table 1 that the terminal mean cluster size in the simulations with different initial conditions is approximately constant (500). The initial conditions that resulted in this cluster size are compared with the scaling law of Eq. (22) in Fig. 4, where circles represent the DSMC values and the dashed line represents the scaling law. Figure 4 suggests that the power-law relationship, Eq. (22), holds for the stagnation pressure P_0 and throat diameter d. The estimated value of the exponent q obtained from the DSMC calculations of 0.85 is close to the experimental value of 0.8.

Another interesting result is found by the analysis of cluster growth along the centerline. Figure 5 represents the average cluster size as a function of the distance from the throat, normalized by the throat radius and the mean terminal cluster size (see Table 1). It is seen in the figure that cluster growth only weakly depends on the initial conditions, which is also consistent with Hagena's derivation of the second scaling law, Eqs. (23) and (24), which assumed isentropic expansion. The small differences between the curves can be attributed to the nonlinear effects of the coupled evaporation and condensation processes accompanying the growth of clusters. Note that in all of these cases, the degree of condensation is not significant enough to change the flowfield. Note also that the first scaling law of Hagena, Eq. (22), is purely empirical and is not based on a model of isentropic expansion.

Similar calculations are conducted to test the second scaling law, Eqs. (23) and (24). Table 2 and Fig. 6 represent the results. It is seen in the figure that the power-law relation between the stagnation pressure and temperature holds for the simulated data, while the estimated value of -2.48 of the temperature exponent agrees with the prediction by Eqs. (23) and (24) interval between -2.5 and -2.25. Figure 7 shows the growth of cluster size along the centerline for the second considered case. Although the normalized curves are

similar in shape, it is noticeable that the higher the stagnation temperature is, the more the nucleation region moves downstream. This shift can be attributed to the higher evaporation rates of small clusters at the higher temperature. Concluding this subsection, we can state that the developed computational scheme reproduces correctly the experimentally based scaling laws. Moreover, these simulations represent the first rigorous DSMC numerical validation of Hagena's scaling laws, free of concerns raised about experimental uncertainties of his work.[18]

C. Rocket Plume Cases

The developed kinetic model based on the DSMC method is applied in this work to the study of condensation processes in plumes expanding into vacuum from a rocket engine with a thrust level of several thousand newtons. Under these conditions condensation is expected to occur for the low-Earth-orbit conditions. The example plume considered here is from the Progress spacecraft main engine firing at an altitude of 300 km, with stagnation pressure of approximately 350 KPa and stagnation temperature about 3800 K. The pressure and temperature contours obtained by solving Navier–Stokes equations[37] without condensation of the plume flow are shown in Figs. 8 and 9. Note that the dashed line shows the inflow starting surface for the DSMC computations, created from a single pressure contour line of Navier–Stokes solution in the undersaturated region. The species mole fraction and vibrational characteristic temperature in the noncondensation plume are shown in Table 3.

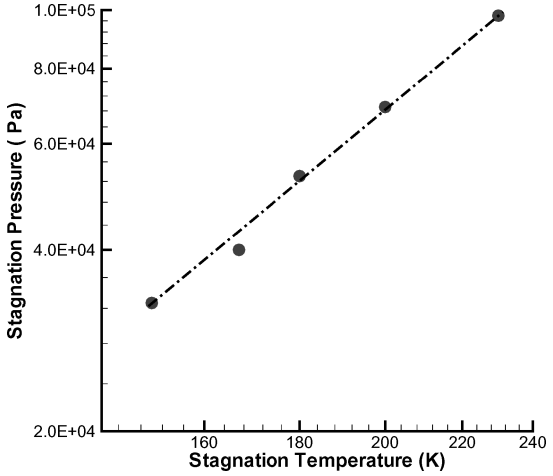

Fig. 6 Comparison of DSMC simulation conditions (●) with the scaling law, Eqs. (23) and (24) (–·–·–·), $d = 0.14$ mm.

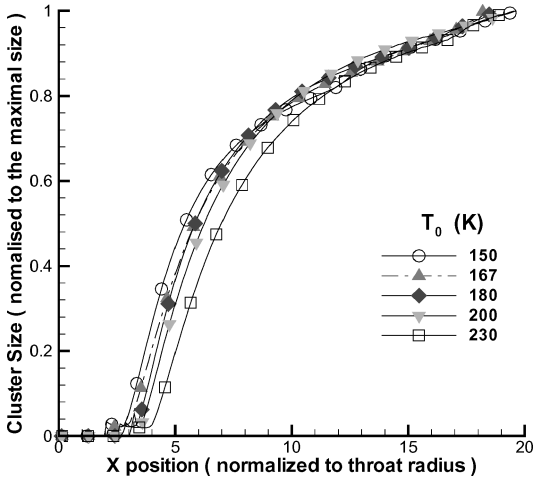

Fig. 7 Cluster growth along the centerline of the DSMC simulations, with the conditions shown in Fig. 6.

Figure 10 shows the local gas Knudsen-number distribution along the plume centerline. The Knudsen number is defined as the ratio of local mean free path to the nozzle-throat diameter. We can see that most of the simulation region is in the transitional and rarefied regimes, and the use of a continuum approach in these regions can result in errors. Because the DSMC method is appropriate for the rarefied and transitional regime, we believe that DSMC method will provide generally more accurate results as compared with the continuum method. However, the flow inside the starting surface is in a continuum region with a typical Knudsen number $\leq 10^{-3}$, and the use of the DSMC method in this region would be impractical. Thus, the DSMC simulation of the supersonic plume flow with condensation begins from an imposed starting surface, which is composed of 480 segments, each with a number density of approximately 4.5×10^{21} molecules/m^3.

The location of the starting surface is indicated by a dashed line in Figs. 8, 9, and 11–13. Based on the continuum single-phase plume solution, the degree of water-vapor supersaturation $S = P/P_s(T)$ was calculated and shown in Ref. 14. The variables P and $P_s(T)$ are the water-vapor pressure and water-vapor saturation pressure,[38] respectively, at the local gas temperature. In the inner region of the starting surface, the degree of water-vapor saturation is less than unity, which means that the water vapor is in an unsaturated state. In the region downstream of the starting surface, the degree of water-vapor saturation increases dramatically because the saturation pressure decreases exponentially with temperature. Therefore, no condensation flow will appear in the region upstream of the starting surface, and condensation is only possible in the downstream of the starting surface.

Classical homogeneous nucleation theory is applied to the plume flowfield to obtain the initial nuclei distribution. The nuclei are created spontaneously with the average local gas temperature, velocity, and the critical size according to the local degree of supersaturation

Table 3 Plume species, mole fractions, and vibrational characteristic temperatures Θ_v

Species	Mole fraction	Θ_v, K
H	0.0093	——
N_2	0.2675	2256
NO	0.0012	2719
H_2	0.1905	6159
CO	0.1896	3103
CO_2	0.0524	945
H_2O	0.2895	2290

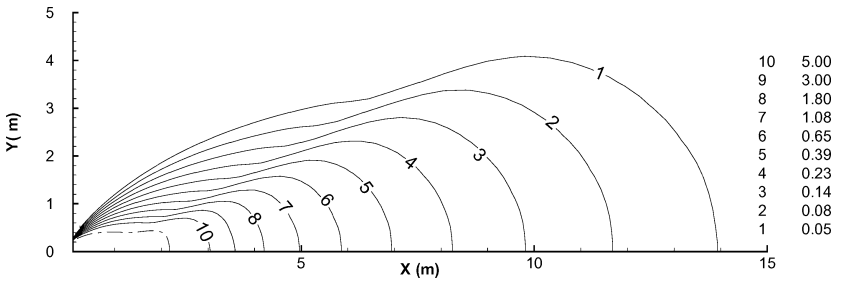

Fig. 8 Pressure contours (Pa) for the Progress spacecraft main engine plume in low Earth orbit; condensation is neglected. The Navier–Stokes solver is used to obtain the starting surface (–·–·–·) for the DSMC calculation downstream.

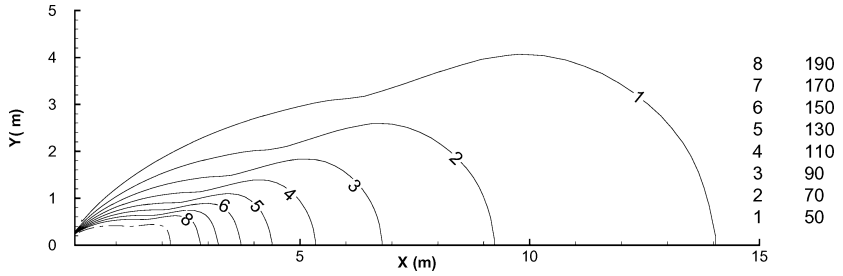

Fig. 9 Temperature contours (K) for the Progress spacecraft main engine plume in low Earth orbit; condensation is neglected. The Navier–Stokes solver is used to obtain the starting surface (–·–·–·) for the DSMC calculation downstream.

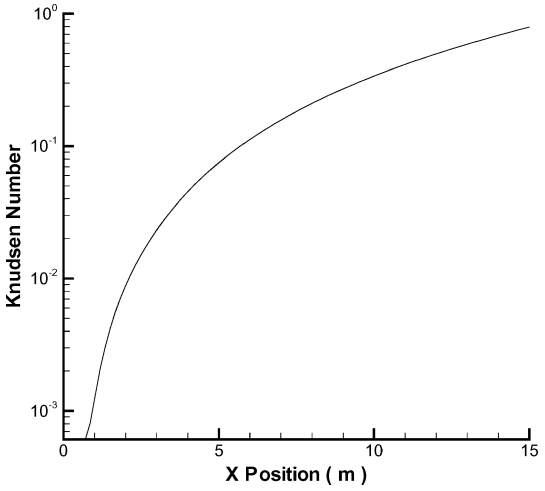

Fig. 10 Gas Knudsen number along the plume centerline for the low Earth orbit; condensation is neglected.

S. Various nuclei originally created per time step would be transported downstream, leading to condensation, evaporation, and collisional processes, which will affect the flowfield.

Based on the modified SMILE code, the developed axial-symmetric DSMC scheme is applied using a computational domain of 5×15 m with 120×360 cells in the radial and axial directions, respectively. Each cell can be divided into up to 100 subcells according to the flow gradients obtained during the simulation. The grid size is determined by the mean free path, and a time step of 2.0×10^{-7} s was used to ensure that the displacement of simulated molecules per time step is less than one cell size. Because the cluster number density is much smaller than gas-species number density, a cluster-species weighing factor of 5.0×10^{-6} is chosen to have enough simulated particles to represent clusters,[7] whereas all of the other species have a unity-species weighting factor. Fnum, the number of real molecules or clusters represented by a simulated particle, is 1.0×10^{15} and 5.0×10^{9} for gas species and cluster, respectively. To decrease the computational cost, radial weights are used for distributing the number of simulated molecules evenly in the radial direction for all species. About 2,100,000 simulated gas molecules and 1,200,000 simulated cluster molecules are used at steady state to simulate the condensation coupled plume flow.

In the DSMC simulation, first the noncondensation flow was modeled to the steady state. Classical nucleation theory is then applied to the plume flowfield to obtain the initial nuclei distribution as was explained in detail in the preceding section. The nuclei are created in the nucleation region based on the gas macroscopic parameters, which are recalculated every 5000 steps during the simulation. During each time step, all clusters can undergo condensation, reflection, and evaporation processes. After the 24,000th time step beyond the creation of the first nuclei, the condensation coupled flow is assumed to have reached steady state. The results are then sampled up to the 400,000th time step.

The cluster number density contours in the steady state are shown in Fig. 11, where the maximum cluster number density indicates the onset of the condensation. We can see that the onset of condensation begins at approximately 3 m beyond the exit of the nozzle, which is a distance of about 40 times the nozzle throat diameter. We will designate this region of the flow as the nucleation region. The cluster number density in the nucleation region is of the order of $10^{15}/\text{m}^3$, which is approximately six orders of magnitude smaller than that of the local gas species. The cluster number density is seen to decrease downstream, as well as in the radial direction, mainly because of flow expansion.

Contours of average cluster size in the steady state are shown in Fig. 12. The average cluster size in the nucleation region is about 10, approximately the same cluster size measured in the nucleation region in the experiments discussed in Ref. 39. Starting from the nucleation region, the average size of the clusters increases steadily downstream due to the condensation process. The characteristic shape of the curves can be explained as follows. Inside the core flow, where the clusters experience more frequent collisions with gas monomers, the average cluster size contours follow the number density contours depicted in Fig. 11. Outside of the denser region, the cluster size contour lines are almost consistent with the straight flow streamlines because of lack of collisions in the rarefied region. Figure 14 compares average cluster and gas velocities along the radial direction at the distance of 10 m from the main engine nozzle exit, which shows that there is almost no velocity slip between the cluster and the gas. Thus, the magnitude of relative velocity between clusters and gas would approximately equal to the gas thermal velocity. Beyond the computational domain, because the relative velocity is rather low as a result of the low temperature and the vapor number density is more than three orders of magnitude lower than the nucleation region, the collision probability between cluster and gas species will be much smaller, even though the cluster size has increased. We can conclude that the maximum cluster size is around 500 in the computational domain. The small cluster sizes and fraction of clusters hardly impact the gas macroparameters, such as pressure, temperature, and density. Comparison of the noncondensation and condensation-coupled flowfields showed no difference, as can be expected.

Contours of average cluster temperature in the steady state are shown in Fig. 13. We can see that the average cluster temperature decreases along the expansion directions because of the combined effects of condensation heating, evaporation, and collisional coolings. Comparing Fig. 13 with Fig. 9, we can see that the average cluster temperature is higher than the local gas temperature, thus thermal nonequilibrium exists in the condensation flow, which will be shown more explicitly in Fig. 15.

The preceding numerical simulation was based on the CNT nucleation rate, Eq. (6), referred to here as the CNT rate. However, because of the uncertainties of small cluster surface tension and free energy at low temperatures, the error in CNT rate might be high. For example, decreasing the surface tension of water by 25% can increase the nucleation rate by more than 10 orders of magnitude.[40] Based on an extended set of experimental data, Wolk et al.[27] found that CNT rate should be corrected as the function of temperature and suggested an empirical rate equation for water as follows:

$$J_{\text{CER}} = J_{\text{CNT}} \exp[-27.56 + (6.5 \times 10^3)/T] \qquad (25)$$

The corrected nucleation rate from the preceding equation is referred to as the CER rate in this work. In the rocket plume case, the

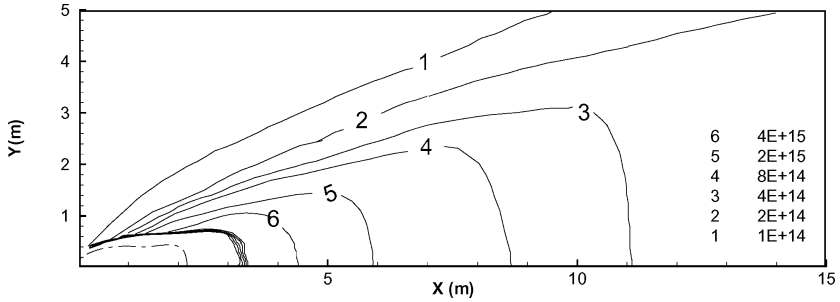

Fig. 11 Cluster number density contours (per m^3) in a main engine plume at low-Earth-orbit conditions, obtained by the DSMC method.

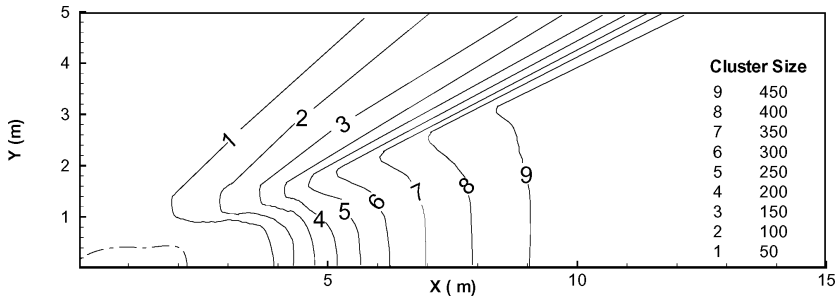

Fig. 12 Average cluster size in a main engine plume at low-Earth-orbit conditions, obtained by the DSMC method.

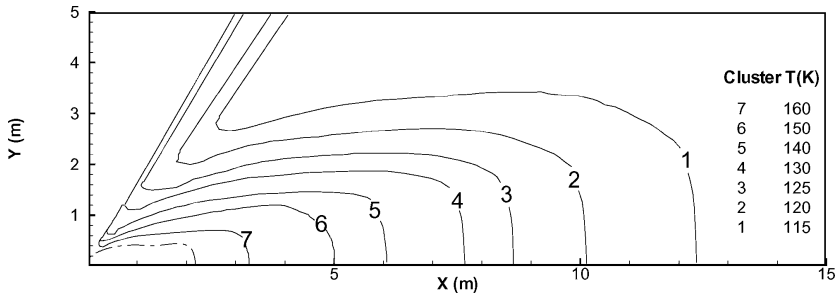

Fig. 13 Average cluster temperature (K) in the main engine plume at the low-Earth-orbit conditions, obtained by the DSMC method.

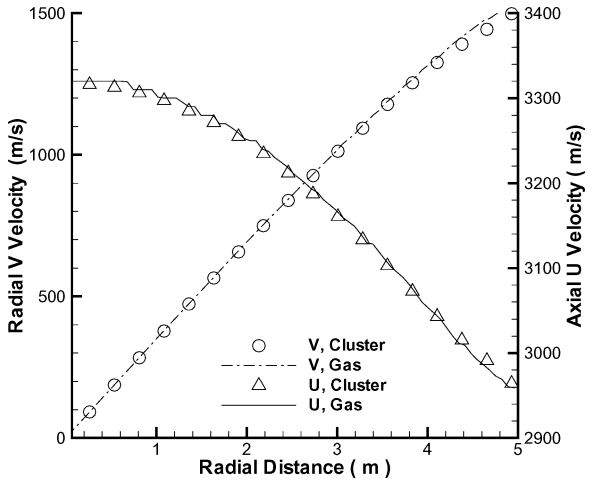

Fig. 14 Average cluster and gas velocities along the radial direction at the distance of 10 m from the main-engine nozzle exit, obtained by the DSMC method.

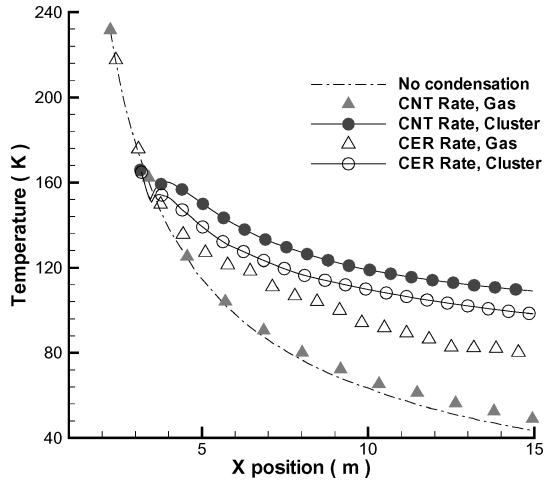

Fig. 15 Comparison of gas and cluster temperatures for two nucleation rates along the plume centerline for low-Earth-orbit conditions.

magnitude of the CER rate is approximately three orders larger than the CNT rate because the flow temperature in the nucleation region is about 180 K. To study the impact and sensitivity of the nucleation rate on the condensation flow, we compared the simulated flows obtained with the CNT and CER rates along the plume center line.

First, the average cluster temperature is compared with the gas temperature for the two nucleation rates along the center line in Fig. 15. Because the flow translational temperature equals the cluster internal temperature within the nucleation region, we can state that in both cases the nucleation process proceeds in thermal equilibrium. The increase of cluster temperature near the nucleation region can be attributed to more significant energy gains of freshly nucleated small clusters in the sticking collisions, when the cluster mass is comparable to the monomer mass. Beyond the nucleation region, the translational temperature in the plume quickly decreases while the decrease of the cluster internal temperature is rather slow, indicating that thermal nonequilibrium persists in this domain. The

differences exist clearly for the two nucleation rates. First, the gas temperature in CNT rate is almost the same as that of noncondensation flow. However, condensation with the CER rate leads to the increase of gas temperature compared with noncondensation flow. Second, clusters in CNT rate have a higher internal temperature than those in CER rate. Finally, the higher CER rate leads to a smaller degree of thermal nonequilibrium than lower CNT rate. The differences in the simulation results can be explained from the cluster size and number density as follows.

The average cluster size of the two nucleation rates is compared along the centerline in Fig. 16. For the CNT rate being lower, the growth of cluster occurs in a range of approximately 15 m; however, for the CER rate being higher, cluster growth is completed by approximately 5 m. The terminal cluster size for CNT rate is approximately 500; however, for the CER rate it is less than 80. Thus, for the larger nucleation rate the condensation process will be faster, and clusters will obtain less condensation heat from the flow because of their smaller sizes. For this case, cluster internal temperatures obtained with the CER rate are usually lower than those obtained with the CNT rate. The cluster number density of the two nucleation rates is compared along the centerline in Fig. 17. We can see that the cluster number density decreases with distance from the nozzle, which is similar for both rates. Because gas molecules have a greater chance to collide with hot clusters in the simulation that uses the CER rate, as a result of about three orders of magnitude larger cluster number density, the energy transfer between the cluster and gas is more efficient for the higher nucleation rate. The gas in the CER rate simulation is heated by the hotter clusters during the nonsticking collision process, whereas this does not occur in the CNT rate simulations due to the lack of collisions between clusters and foreign molecules. Thus, we observe that only in the CER rate simulations is the gas temperature higher than in the noncondensation case. Compared with the CNT rate, the CER rate simulations has a relatively higher gas temperature and lower cluster temperature. This indicates that increasing the nucleation rate increases the degree of thermal equilibrium.

The average water-vapor number density of the two nucleation rates is compared along the centerline in Fig. 18. For the CNT rate, the consumption of water-vapor number density due to the condensation process can be neglected by comparing with the noncondensation flow. However, for the CER rate the dramatic decrease of water-vapor number density near the nucleation region is mainly due to the high nucleation rate. The larger nuclei creation process consumes more monomers and leads to a stronger condensation process, which

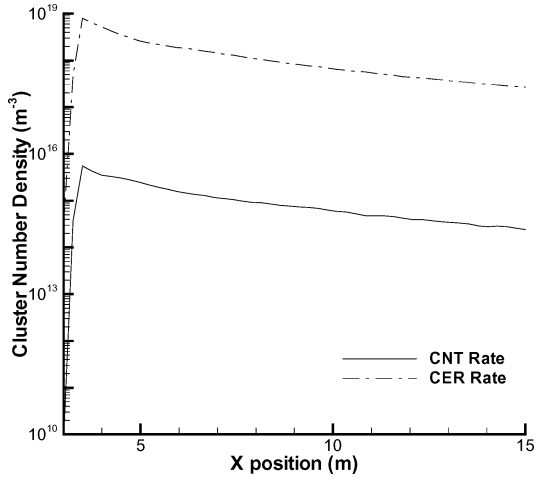

Fig. 17 Comparison of cluster number densities for two nucleation rates along the plume centerline for low-Earth-orbit conditions.

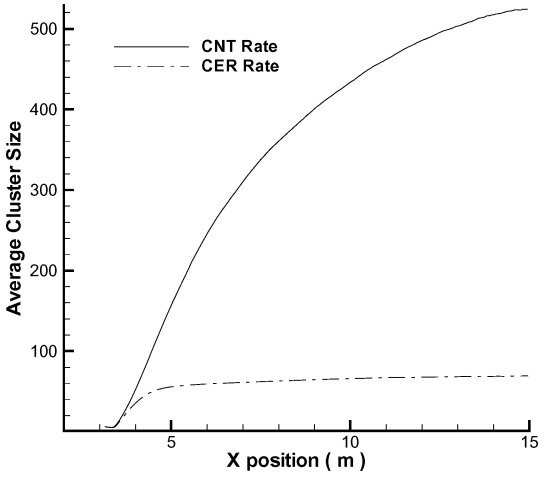

Fig. 16 Comparison of cluster sizes for two nucleation rates along the plume centerline for low-Earth-orbit conditions.

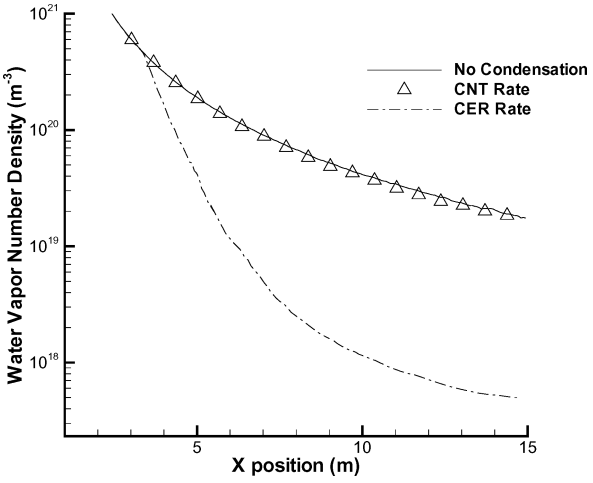

Fig. 18 Comparison of water-vapor number densities for two nucleation rates along the plume centerline for low-Earth-orbit conditions.

Table 4 Comparison of particle number density (ND, molecules/m^3) and collision frequencies (CF, collisions/m^3/s) between CNT and CER rates at 4, 8, and 15 m away from the nozzle exit along the core flow[a]

	4 m		8 m		15 m	
Flow condition	CNT	CER	CNT	CER	CNT	CER
Temperature, K	140.3	143.5	80.1	103.3	49.6	79.7
Mean cluster size	52	35	360	63	524	69
Cluster ND	3.5×10^{15}	5.18×10^{18}	9.2×10^{14}	1.08×10^{18}	2.5×10^{14}	2.72×10^{17}
H_2O ND	3.12×10^{20}	1.68×10^{20}	6.44×10^{19}	2.53×10^{18}	1.66×10^{19}	4.9×10^{17}
Molecular ND	1.05×10^{21}	9.07×10^{20}	2.27×10^{20}	1.60×10^{20}	6.07×10^{19}	4.25×10^{19}
Molecule–molecule CF	9.46×10^{25}	7.0×10^{25}	3.3×10^{24}	1.88×10^{24}	1.88×10^{23}	1.17×10^{23}
Molecule–cluster CF	1.1×10^{21}	1.0×10^{24}	1.7×10^{20}	5.0×10^{22}	1.26×10^{19}	3.14×10^{21}
Cluster–cluster CF	3.66×10^{15}	6.23×10^{22}	6.9×10^{14}	3.4×10^{20}	5.18×10^{13}	2.0×10^{19}
K_c[b]	4.18×10^{-7}	4.81×10^{-3}	3.0×10^{-7}	1.26×10^{-4}	8.29×10^{-8}	2.94×10^{-5}

[a]A value of surface tension, $\sigma = 0.074$ N/m for a water cluster was used in all simulations.
[b]K_c represents the average number of cluster–cluster collisions per cluster during one time step.

at the same time consumes more water vapor monomers. Note that the smaller water-vapor number density of the CER rate in Fig. 18 causes a smaller average cluster size, shown in Fig. 16. For the CNT rate, the condensation process is essentially completed by 5 m, beyond that the growth of clusters is slow, and the decrease of the vapor number density is mainly a result of the expansion process.

Finally, we compare the frequency of molecule–molecule (M–M), molecule–cluster (M–C), and cluster–cluster (C–C) collisions between CNT and CER rate at the location 4, 8, and 15 m away from the nozzle exit along the core plume in Table 4. The comparison shows that the number of molecule–molecule collisions is at least three orders of magnitude greater than that of cluster–cluster collisions because of a larger molecule number density. The number of cluster–cluster collisions per cluster during one time step is also shown in Table 4. Because the coalescence probability depends on cluster–cluster collisions, it can be concluded that the potential contribution of coalescence to the cluster growth process is indeed negligible in this work.

VII. Conclusions

Microscopic nucleation, condensation, nonsticking collisions, and evaporation models, consistent with CNT, are developed and integrated into a DSMC code to simulate condensation in rocket plumes. Comparison of three one-dimensional simulation test cases with analytic solutions are used to validate the numerical algorithms for the microscopic models implemented in DSMC. Numerical and microscopic model validation is further achieved by comparison with Hagana's scaling laws. The DSMC condensation coupled flow solutions, including cluster number density, size, and temperature, are obtained for the first time.

The classical nucleation rate is corrected based on an empirical equation, which leads to a three order of magnitude larger rate than the original CNT rate in the rocket plume case. Based on these two rates, cluster size, temperature, number density, and gas temperature are compared along the core flow. Our DSMC simulation result suggests that condensation phenomenon does exist in the rocket plume and that thermal nonequilibrium exists among clusters and gas. It also shows that the degree of condensation in the flow strongly depends on the nucleation rate, in terms of cluster number density, size, temperature, gas temperature, and density, the region where condensation will occur, and degree of thermal nonequilibrium. A higher nucleation rate causes condensation to occur at a shorter distance from the nozzle and creates a stronger condensation shock.

The use of the corrected nucleation rate is not the only possibility to improve the accuracy of the DSMC-based kinetic approach. Another promising direction would avoid the use of CNT could be based on molecular dynamics[9] characterization of possible channels of monomer and cluster reactions, including the ternary collisions of the monomers and the following implementation of these reactions in DSMC. This approach will be considered in future work.

Acknowledgments

The research performed at the Pennsylvania Sate University was supported by Air Force Office of Scientific Research Grant F49620-02-1-0104 administered by Mitat Birkan and Army Research Office Grant DAAD19-02-1-0196 administered by David Mann. Special thanks are extended to M. Ivanov of the Institute of Theoretical and Applied Mechanics, Russia, for the use of the original SMILE code.

References

[1]Abraham, F. F., *Homogeneous Nucleation Theory*, Academic Press, New York, 1974.

[2]McDonald, J. E., "Homogeneous Nucleation of Vapor Condensation I. Thermodynamic Aspects," *American Journal of Physics*, Vol. 30, No. 12, 1962, pp. 870–877.

[3]McDonald, J. E., "Homogeneous Nucleation of Vapor Condensation II. Kinetic Aspects," *American Journal of Physics*, Vol. 31, No. 1, 1963, pp. 31–41.

[4]Wu, B. J. C., "Possible Water Vapor Condensation in Rocket Exhaust Plumes," *AIAA Journal*, Vol. 13, No. 6, 1975, pp. 797–802.

[5]Perrel, E. R., Erickson, W. D., and Candler, G. V., "Numerical Simulation of Nonequilibrium Condensation in a Hypersonic Wind Tunnel," *JSME International Journal, Series B*, Vol. 39, No. 2, 1996, pp. 277–283.

[6]Masuda, W., Satoh, M., and Yamada, H., "Effects of Water Vapor Condensation on the Performance of Supersonic Flow Chemical Oxygen-Iodine Laser," *Journal of Thermophysics and Heat Transfer*, Vol. 10, No. 2, 1996, pp. 273–278.

[7]Bird, G. A., *Molecular Gas Dynamics and the Direct Simulation of Gas Flows*, Oxford Science Publications, New York, 1994.

[8]Luk'yanchuk, S., Marine, W., Anisimov, S. I., and Simakina, G. A., "Condensation of Vapor and Nanoclusters Formation Within the Vapor Plume, Produced by Ns-Laster Ablation of Si, Ge, and C," *Proceedings of the SPIE*, Vol. 3618, 1999, pp. 434–452.

[9]Venkatesh, R., Lucchese, R. R., Marlow, W. H., and Schulte, J., "Thermal Collision Rate Constants or Small Nickel Clusters of Size 2-14 Atoms," *Journal of Chemical Physics*, Vol. 102, No. 19, 1995, pp. 7683–7699.

[10]Oxtoby, D. W., "Nonclassical Nucleation Theory: An Exactly Soluble Model," *Physica Scripta T*, Vol. T49A, 1993, pp. 65–69.

[11]Knuth, E., "Dimer-Formation Rate Coefficients from Measurements of Terminal Dimer Concenrations in Free-Jet Expansions," *Journal of Chemical Physics*, Vol. 66, No. 8, 1977, pp. 3515–3525.

[12]Knuth, E., "Size Correlations for Condensation Clusters Produced in Free-Jet Expansions," *Journal of Chemical Physics*, Vol. 107, No. 21, 1997, pp. 9125–9132.

[13]Briehl, B., and Urbassek, H. M., "Monte Carlo Simulation of Growth and Decay Processes in a Cluster Aggregation Source," *Journal of Cacuum Science & Technology A*, Vol. 17, No. 1, 1999, p. 256.

[14]Zhong, J., Gimelshein, S. F., Zeifman, M. I., and Levin, D. A., "Modeling of Homogeneous Condensation in Supersonic Plumes with the DSMC Method," AIAA Paper 2004-0166, Jan. 2004.

[15]Hagena, O. F., and Obert, W., "Cluster Formation in Expanding Supersonic Jets: Effect of Pressure, Temperature, Nozzle Size, and Test Gas," *Journal of Chemical Physics*, Vol. 56, No. 5, 1972, pp. 1793–1802.

[16]Zeifman, M. I., Zhong, J., and Levin, D. A., "A Hybrid MD-DSMC Approach to Direct Simulation of Condensation in a Supersonic Jets," AIAA Paper 2004-2586, June 2004; also *Physics of Fluids* (submitted for publication).

[17]Yasuoka, K., and Matsumoto, M., "Molecular Dynamics of Homogeneous Nucleation in the Vapor Phase. I. Lennard-Jones Fluid," *Journal of Chemical Physics*, Vol. 109, No. 19, 1998, pp. 8463–8470.

[18]Haberland, H., "3 Experimental Methods," *Clusters of Atoms and Molecules I: Theory, Experiment, and Clusters of Atoms*, Springer-Verlag, Berlin, 1995, pp. 207–252.

[19]Itkin, A. L., and Kolesnichenko, E. G., *Microscopic Theory of Condensation in Gases and Plasma*, World Scientific, Singapore, 1997.

[20]Schenter, G. K., Kathmann, S. M., and Garrett, B. C., "Variational Transition State Theory of Vapor Phase Nucleation," *Journal of Chemical Physics*, Vol. 110, No. 16, 1999, pp. 7951–7959.

[21]Lothe, J., and Pound, G. M., "Reconsiderations of Nucleation Theory," *Journal of Chemical Physics*, Vol. 36, April 1962, pp. 2080–2085.

[22]Reiss, H., Katz, J. I., and Cohen, E. R., "Translation-Rotation Paradox in the Theory of Nucleation," *Journal of Chemical Physics*, Vol. 48, No. 12, 1968, pp. 5553–5560.

[23]Sharaf, M. A., and Dobbins, R. A., "A Comparison of Measured Nucleation Rate with the Predictions of Several Theories of Homogeneous Nucleation," *Journal of Chemical Physics*, Vol. 77, No. 3, 1982, pp. 1517–1526.

[24]Zahoransky, R. A., Hoschele, J., and Steinwandel, J., "Formation of Argon Clusters by Homogeneous Nucleation in Supersonic Shock Tube Flow," *Journal of Chemical Physics*, Vol. 103, No. 22, 1995, pp. 9038–9044.

[25]Senger, B., Schaaf, P., Corti, D. S., Bowles, R., Pointu, D., Voegel, J. C., and Reiss, H., "A Molecular Theory of the Homogeneous Nucleation Rate. II. Application to Argon Vapor," *Journal of Chemical Physics*, Vol. 110, No. 13, 1999, pp. 6438–6450.

[26]Yasuoka, K., and Matsumoto, M., "Molecular Dynamics of Homogeneous Nucleation in the Vapor Phase. II. Water," *Journal of Chemical Physics*, Vol. 109, No. 19, 1998, pp. 8451–8462.

[27]Wolk, J., Strey, R., Heath, C. H., and Wyslouzil, B. E., "Empirical Function for Homogeneous Water Nucleation Rate," *Journal of Chemical Physics*, Vol. 117, No. 10, 2002, pp. 4954–4960.

[28]Wolk, J., and Strey, R., "Homogeneous Nucleation of H_2O and D_2O in Comparison: the Isotope Effect," *Journal of Physical Chemistry B*, Vol. 105, No. 47, 2001, pp. 11683–11701.

[29]Malakhovskii, A. V., and Ben-Zion, M., "Temporal Evolution of an Argon Cluster During the Process of Its Evaporation," *Chemical Physics*, Vol. 264, No. 1, 2001, pp. 135–143.

[30]Carey, P. V., *Statistical Thermodynamics and Microscale Thermophysics*, Cambridge Univ. Press, Cambridge, England, U.K., 1999.

[31]Ivanov, M. S., Markelov, G. N., and Gimelshein, S. F., "Statistical Simulation of Reactive Rarefied Flows: Numerical Approach and Application," AIAA Paper 98-2669, June 1998.

[32]Erickson, W. D., Mall, G. H., and Prabhu, R. K., "Finite-Rate Water Condensation in Combustion Heated Wind Tunnels," NASA TP, 2833, 1988.

[33]Peters, F., and Meyer, K. A. J., "Measurement and Interpretation of Growth of Monodispersed Water Droplets Suspended in Pure Vapor," *International Journal of Heat Mass Transfer*, Vol. 38, No. 17, 1995, pp. 3285–3293.

[34]Kolb, C. E., Lyons, R. B., Elgin, J. B., Huffman, R. E., Paulsen, D. E., and McIntyre, A., "Scattered Visible and Ultraviolet Solar Radiation from Condensed Attitude Control Jet Plumes," *Journal of Spacecraft and Rockets*, Vol. 20, No. 4, 1983, pp. 383–389.

[35]"The General Aerodynamic Simulation Program," GASP ver. 4.1, *Computational Flow Analysis Software for the Scientist and Engineer*, User's Manual, Aerosoft, Inc., Blacksburg, VA.

[36]*Tables of Thermal Properties of Gases*, National Bureau of Standards, Circular 564, Nov. 1955.

[37]Drakes, J. A., Swann, D. G., Karabadzhak, G. F., and Plastini, Yu., "DSMC Computations of the Progress-M Spacecraft Retrofiring Exhaust Plume," AIAA Paper 99-0975, Jan. 1999.

[38]Ivarsson, K. I., "Tests with Separated Tables for Water Vapor Saturation Pressure over Ice and Water," HIRLAM Technical Repts. No. 45, Norrkoping, Dec. 2002.

[39]Streletzky, K. A., Zvinevich, Y., Wyslouzil, B. E., and Strey, R., "Controlling Nucleation and Growth of Nanodroplets in Supersonic Nozzles," *Journal of Chemical Physics*, Vol. 116, No. 10, 2002, pp. 4058–4070.

[40]Kathmann, S. M., Schenter, G. K., and Garrett, B. C., "Understanding the Sensitivity of Nucleation Kinetics: A Case Study on Water," *Journal of Chemical Physics*, Vol. 116, No. 12, 2002, pp. 5046–5057.

C. Kaplan
Associate Editor